Electronic Supplementary Material (ESI) for Physical Chemistry Chemical Physics.

Supporting info: The effect of cation size on structure and properties of Ba-based tetragonal tungsten bronzes $Ba_4M_2Nb_{10}O_{30}$ (M=Na, K or Rb) and $Ba_4M_2Ti_2Nb_8O_{30}$ (M=Ca or Sr).

Nora Statle Løndal, Benjamin Albert Dobson Williamson, Julian Walker, Mari-Ann Einarsrud and Tor Grande

Department of Materials Science and Engineering
NTNU Norwegian University of Science and Technology, NO-7491 Trondheim, Norway

Rietveld refinement

Table S1. The details for Rietveld refinement of occupancy for the BMN and BMNT TTB powder samples. For the *Amm*2 and *Cmm*2 structure A2, B1 and B2 sites are split in two, while for the *P*4*bm* structure these are combined.

Site	Atom	Occupancy
A2_1	Ba	1-(1-xA)/2
	M	(1-xA)/2
A2_2	Ba	1-(1-xA)/2
	M	(1-xA)/2
A1	M	xA
	Ba	1-xA
B2_1	Nb	1-(1-xB)/4
	Ti	(1-xB)/4
B2_2	Nb	1-(1-xB)/4
	Ti	(1-xB)/4
B1_1	Ti	xB
	Nb	1-xB
B1_2	Ti	xB
	Nb	1-xB

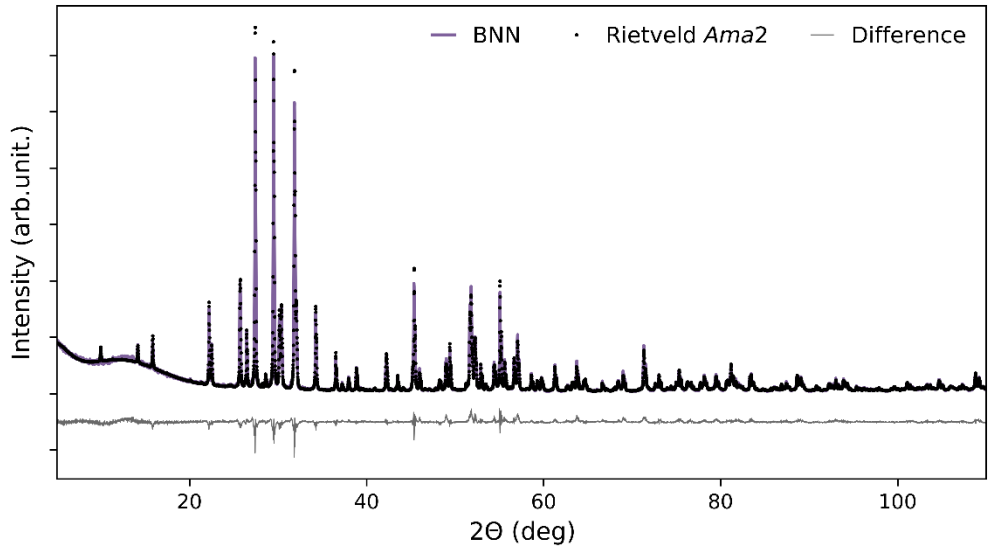

Figure S1: Xray diffractogram BNN with Rietveld refinement towards *Ama*2 space group.

Table S2. Refined *Ama*2 crystal structure of $Ba_4Na_2Nb_{10}O_{30}$. The number of independent parameters that were refined was 167. Unit cell parameters: a = 17.63258(18) Å, b = 35.2036(4) Å and c = 7.98157(7) Å. GOF: 2.08, Rwp: 9.48. Refined parameters are in **bold**.

Site	M_p	Atom	X	Y	Z	Occupancy	B_{eq}
A2_1	8	Ba	**0.9218(12)**	**0.8728(11)**	**0.239(5)**	**0.942(2)**	0.44
		Na				**0.058(2)**	0.44
A2_2	8	Ba	**0.0775(12)**	**0.6224(10)**	**0.237(5)**	**0.942(2)**	0.44
		Na				**0.058(2)**	0.44
A2_3	4	Ba	0.25000	**0.9613(13)**	**0.248(10)**	**0.942(2)**	0.44
		Na				**0.942(2)**	0.44
A2_4	4	Ba	0.75000	**0.5392(13)**	**0.246(9)**	**0.942(2)**	0.44
		Na				**0.058(2)**	0.44
A2_5	4	Ba	0.25000	**0.7883(13)**	**0.246(10)**	**0.942(2)**	0.44
		Na				**0.058(2)**	0.44
A2_6	4	Ba	0.75000	**0.7115(13)**	**0.250(9)**	**0.942(2)**	0.44
		Na				**0.058(2)**	0.44
A1_1	8	Na	**0.503(5)**	**0.7462(16)**	**0.249(19)**	**0.885(5)**	1.6
		Ba				**0.115(5)**	1.6
A1_2	4	Na	0.00000	0.00000	**0.24(3)**	**0.885(5)**	1.6
		Ba				**0.115(5)**	1.6
A1_3	4	Na	0.00000	0.50000	**0.280(12)**	**0.885(5)**	1.6
		Ba				**0.115(5)**	1.6
B1_1	4	Nb	0.75000	**0.125(4)**	0.00000	1	0.42
B1_2	4	Nb	0.25000	**0.375(3)**	0.00000	1	0.42
B1_3	4	Nb	0.75000	**0.875(4)**	0.00000	1	0.42
B1_4	4	Nb	0.25000	**0.625(4)**	0.00000	1	0.42
B2_1	8	Nb	**0.642(4)**	**0.784(3)**	**-0.001(8)**	1	0.42
B2_2	8	Nb	**0.358(5)**	**0.716(2)**	**-0.002(7)**	1	0.42
B2_3	8	Nb	**0.858(5)**	**0.966(2)**	**-0.002(7)**	1	0.42
B2_4	8	Nb	**0.142(5)**	**0.534(2)**	**0.000(7)**	1	0.42
B2_5	8	Nb	**0.432(4)**	**0.821(3)**	**0.000(8)**	1	0.42
B2_6	8	Nb	**0.568(5)**	**0.679(3)**	**-0.001(7)**	1	0.42
B2_7	8	Nb	**0.068(5)**	**0.929(2)**	**0.000(8)**	1	0.42
B2_8	8	Nb	**0.932(5)**	**0.571(2)**	**-0.001(7)**	1	0.42
O1_1	8	O	**0.031(10)**	**0.88(2)**	**-0.02(3)**	1	1.17
O1_2	8	O	**0.968(11)**	**0.625(17)**	**-0.058(15)**	1	1.17
O1_3	4	O	0.25000	**0.01(2)**	**-0.01(5)**	1	1.17
O1_4	4	O	0.75000	**0.49(2)**	**-0.02(5)**	1	1.17
O1_5	4	O	0.25000	**0.24(2)**	**-0.02(6)**	1	1.17
O1_6	4	O	0.75000	**0.26(2)**	**-0.01(6)**	1	1.17
O2_1	8	O	**0.61(3)**	**0.231(14)**	**-0.01(4)**	1	1.17
O2_2	8	O	**0.39(4)**	**0.269(14)**	**-0.02(3)**	1	1.17
O2_3	8	O	**0.893(6)**	**0.023(4)**	**-0.141(13)**	1	1.17
O2_4	8	O	**0.11(3)**	**0.482(13)**	**-0.02(3)**	1	1.17
O2_5	8	O	**0.540(19)**	**0.803(8)**	**-0.06(3)**	1	1.17
O2_6	8	O	**0.46(2)**	**0.694(12)**	**-0.02(4)**	1	1.17
O2_7	8	O	**0.964(16)**	**0.949(6)**	**-0.03(3)**	1	1.17
O2_8	8	O	**0.04(3)**	**0.555(15)**	**-0.04(4)**	1	1.17
O3_1	8	O	**0.68(3)**	**0.166(15)**	**-0.02(3)**	1	1.17
O3_2	8	O	**0.32(3)**	**0.335(18)**	**-0.03(3)**	1	1.17

O3_3	8	O	**0.82(3)**	**0.085(17)**	**-0.02(4)**	1	1.17
O3_4	8	O	**0.18(3)**	**0.415(16)**	**0.00(4)**	1	1.17
O3_5	8	O	**0.668(17)**	**0.838(8)**	**-0.05(2)**	1	1.17
O3_6	8	O	**0.33(3)**	**0.662(15)**	**0.01(4)**	1	1.17
O3_7	8	O	**0.83(3)**	**0.911(14)**	**0.01(4)**	1	1.17
O3_8	8	O	**0.17(3)**	**0.589(14)**	**0.01(3)**	1	1.17
O4_1	8	O	**0.869(12)**	**0.794(4)**	**0.24(5)**	1	1.17
O4_2	8	O	**0.145(11)**	**0.727(5)**	**0.24(6)**	1	1.17
O4_3	8	O	**0.655(9)**	**0.974(5)**	**0.24(5)**	1	1.17
O4_4	8	O	**0.366(13)**	**0.539(4)**	**0.25(6)**	1	1.17
O4_5	8	O	**0.413(9)**	**0.936(4)**	**0.24(5)**	1	1.17
O4_6	8	O	**0.546(9)**	**0.573(5)**	**0.25(5)**	1	1.17
O4_7	8	O	**0.076(10)**	**0.818(5)**	**0.24(5)**	1	1.17
O4_8	8	O	**0.941(10)**	**0.675(5)**	**0.25(5)**	1	1.17
O5_1	4	O	0.75000	**0.867(7)**	**0.24(6)**	1	1.17
O5_2	4	O	0.25000	**0.611(5)**	**0.24(7)**	1	1.17
O6_1	4	O	0.75000	**0.114(7)**	**0.24(6)**	1	1.17
O6_2	4	O	0.25000	**0.366(7)**	**0.25(5)**	1	1.17

Table S3. Refined *Cmm*2 crystal structure of $Ba_4Ca_2Nb_8Ti_2O_{30}$. The number of independent parameters that were refined was 62. Unit cell parameters: a = 17.5251(5) Å, b = 17.5495(5) Å and c = 3.95286(7) Å. GOF: 2.01, Rwp: 11.46. Refined parameters are in **bold**.

Site	M_p	Atom	X	Y	Z	Occupancy	B_{eq}
A2_1	4	Ba	**0.1718(4)**	0.50000	0.50000	**0.959(3)**	0.44
		Ca				**0.041(3)**	0.44
A2_2	4	Ba	0.50000	**0.6712(4)**	0.50000	**0.959(3)**	0.44
		Ca				**0.041(3)**	0.44
A1	4	Ca	0.75000	0.25000	**0.443(4)**	**0.918(7)**	1.6
		Ba				**0.082(7)**	1.6
B1_1	2	Nb	0.00000	0.00000	**0.966(10)**	**0.702(14)**	0.42
		Ti				**0.298(14)**	0.42
B1_2	2	Nb	0.00000	0.50000	**0.969(9)**	**0.702(14)**	0.42
		Ti				**0.298(14)**	0.42
B2_1	8	Nb	**0.8926(4)**	**0.3192(4)**	**0.984(5)**	**0.825(4)**	0.42
		Ti				**0.175(4)**	0.42
B2_2	8	Nb	**0.6807(4)**	**0.3923(4)**	**0.972(4)**	**0.825(4)**	0.42
		Ti				**0.175(4)**	0.42
O1_1	4	O	**0.275(4)**	0.50000	**0.01(3)**	1	1.17
O1_2	4	O	0.50000	**0.782(4)**	**-0.065(15)**	1	1.17
O2_1	8	O	**0.8498(19)**	**0.215(2)**	**0.02(2)**	1	1.17
O2_2	8	O	**0.791(3)**	**0.358(2)**	**0.156(9)**	1	1.17
O3_1	8	O	**0.924(3)**	**0.080(3)**	**0.01(2)**	1	1.17
O3_2	8	O	**0.918(3)**	**0.430(3)**	**0.068(10)**	1	1.17
O4_1	8	O	**0.1033(16)**	**0.2954(14)**	**0.48(3)**	1	1.17
O4_2	8	O	**0.6663(15)**	**0.6234(16)**	**0.49(2)**	1	1.17
O5_1	2	O	0.00000	0.50000	**0.40(3)**	1	1.17
O5_2	2	O	0.50000	0.50000	**0.45(5)**	1	1.17

Dielectric spectroscopy

Table S4. Detailed heating program for impedance spectroscopy of BMN and BMNT materials.

Compound	Measurement	Heating program
BNN	1st set 2nd heating:	30-280 °C (steps of 50 °C), 300-400 °C (every 20 °C)
	2nd set 2nd heating:	400-520 °C, 580-600 °C (steps of 20 °C) and 520-580 °C (steps of 5 °C)
BKN	2nd heating:	30 °C, 50-250 °C (steps of 50 °C), 250-290 °C (steps of 10 °C), 290-330 °C (steps of 2 °C) and 340-360 °C (steps of 20 °C)
BRN	2nd heating:	30 °C, 50-200 °C (steps of 50 °C), 200-230 °C, 360-395 (steps of 5 °C) and 230-360 °C (steps of 2 °C)
BCNT	2nd heating:	30-70 °C, 120-400 °C (steps of 10 °C), 70-80 °C, 110-120 °C (steps of 5 °C) and 80-110 °C (steps of 2 °C).
BSNT	1st set 1st cycle:	25°C, 50-400 (steps of 50 °C), 25°C
	1st set 2nd heating:	30, 50-200 (steps of 10 °C), 200-400 (steps of 20 °C)
	1st set 2nd cooling:	400-25 (steps of 25 °C)
	2nd set 1st cycle:	25°C, 50-400 (steps of 50 °C), 25°C
	2nd set 2nd heating:	30-70 °C, 120-200 °C (steps of 10 °C), 70-80 °C, 110-120 °C (steps of 5 °C), 80-110 °C (steps of 2 °C) 200-400 °C (steps of 20 °C)
	2nd set 2nd cooling:	400-25 (steps of 25 °C)

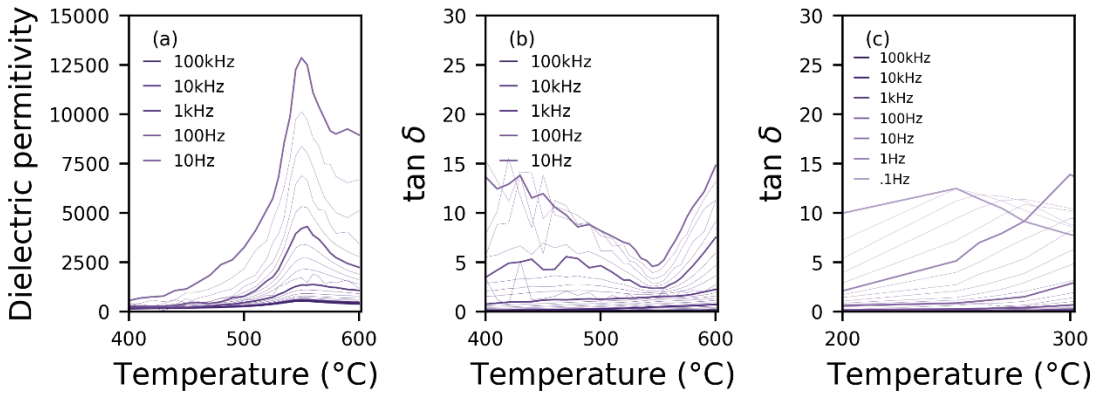

Figure S2: Dielectric spectroscopy data as function of temperature for $Ba_4Na_2Nb_{10}O_{30}$. Dielectric permittivity (a) and tan δ (b) in the frequency range 1-100 kHz between 400 and 600°C displays the ferroelectric transition at 550 °C. A minor feature is present in tan δ in the range 0.1-100 kHz between 200 and 300 °C (c) corresponding to the temperature at which the ferroelastic transition in BNN is expected.

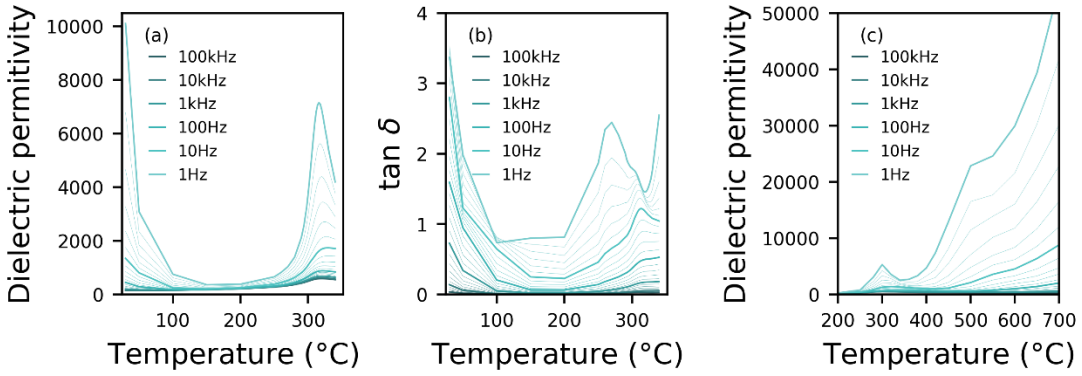

Figure S3: Dielectric spectroscopy data as function of temperature for $Ba_4K_2Nb_{10}O_{30}$. Dielectric permittivity (a) and tan δ (b) in the frequency range 1-100 kHz between 25 and 350°C displays the ferroelectric transition at 320 °C. A second relaxation is present in the dielectric permittivity above the ferroelectric transition at about 500 °C (c).

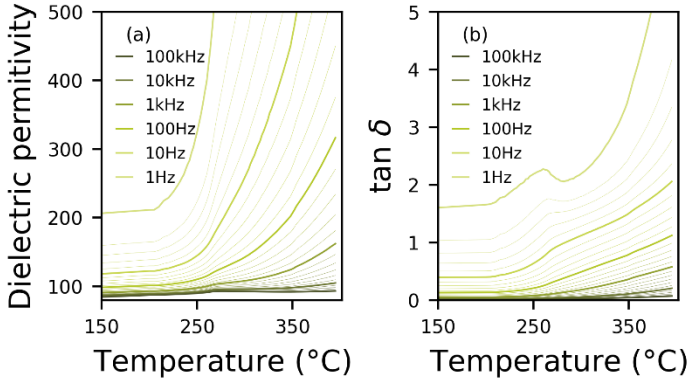

Figure S4: Dielectric spectroscopy data as function of temperature for $Ba_4Rb_2Nb_{10}O_{30}$. Dielectric permittivity (a) and tan δ (b) in the frequency range 1-100 kHz between 150 and 400°C displays the subtle ferroelectric transition at 270 °C.

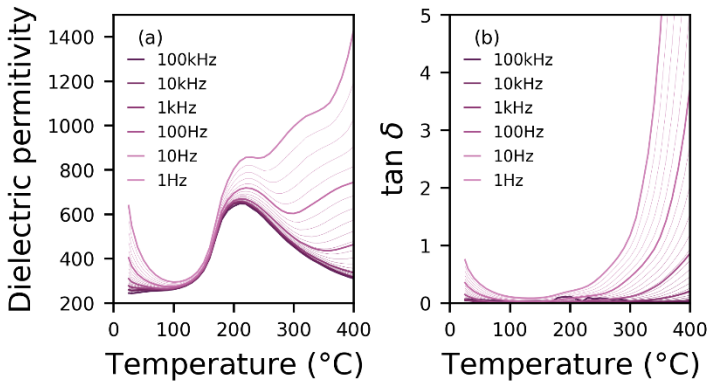

Figure S5: Dielectric spectroscopy data as function of temperature for $Ba_4Ca_2Nb_8Ti_2O_{30}$. Dielectric permittivity (a) and tan δ (b) in the frequency range 1-100 kHz between 25 and 400°C displays the ferroelectric transition at 210 °C.

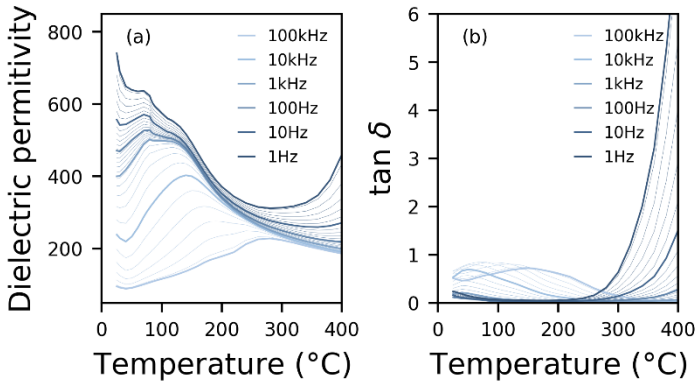

Figure S6: Dielectric spectroscopy data as function of temperature for $Ba_4Sr_2Nb_8Ti_2O_3$. Dielectric permittivity (a) and tan δ (b) in the frequency range 1-100 kHz between 25 and 400°C displays a broad frequency dispersion of the peak permittivity.

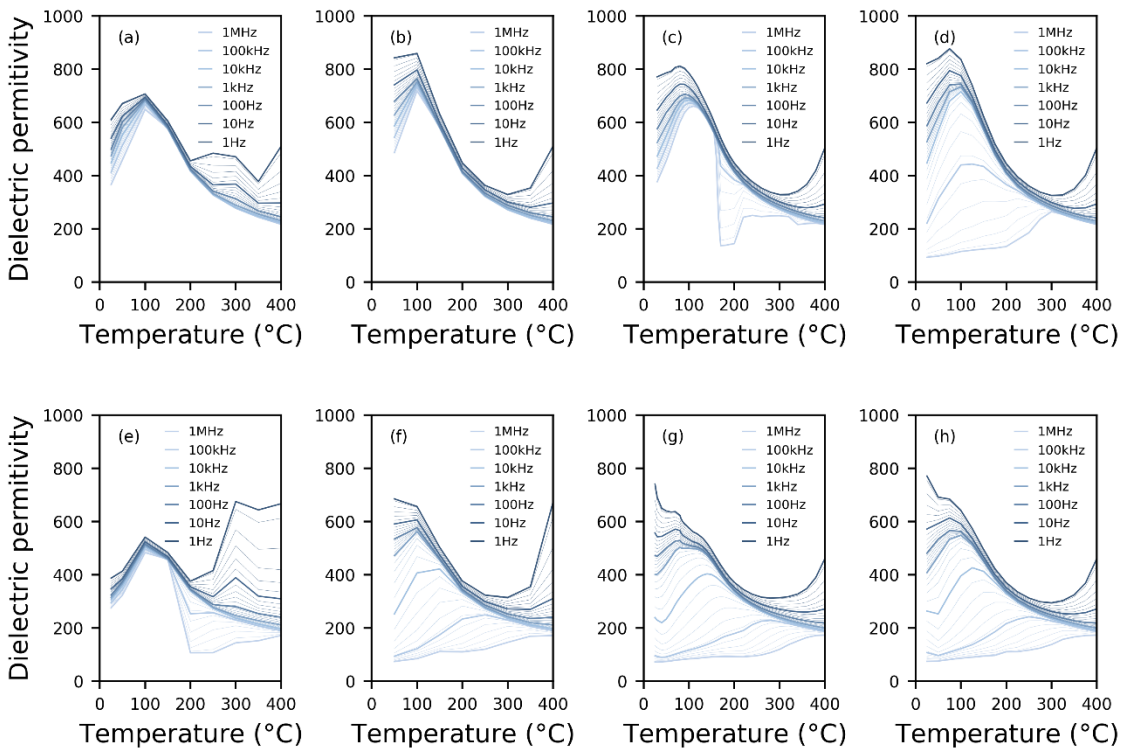

Figure S7: Dielectric permittivity as function of temperature for $Ba_4Sr_2Nb_8Ti_2O_3$. Dielectric permittivity in the frequency range 1-100 kHz between 25 and 400°C is displayed for the first (a-d) and second (e-h) set of measurements. In each set of measurements, the sample is heated (a, c, e and g) and cooled (b, d, f and h) two consecutive times.

DSC

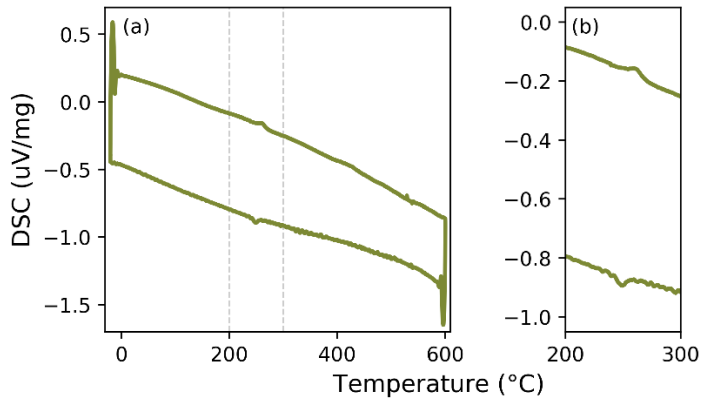

Figure S8: Differential scanning calorimetry as function of temperature for $Ba_4Rb_2Nb_{10}O_{30}$. Endothermic peaks are observed at 250 and 260 °C on heating and cooling, respectively.

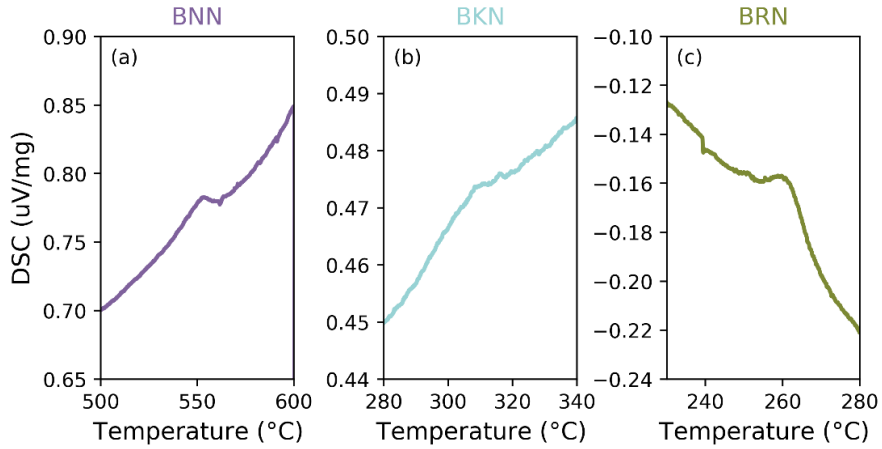

Figure S9: Differential scanning calorimetry as function of temperature. Endothermic peaks are observed for (a) $Ba_4Na_2Nb_{10}O_{30}$ at 550 °C, (b) $Ba_4K_2Nb_{10}O_{30}$ at 310 °C and (c) $Ba_4Rb_2Nb_{10}O_{30}$ at 260 °C.

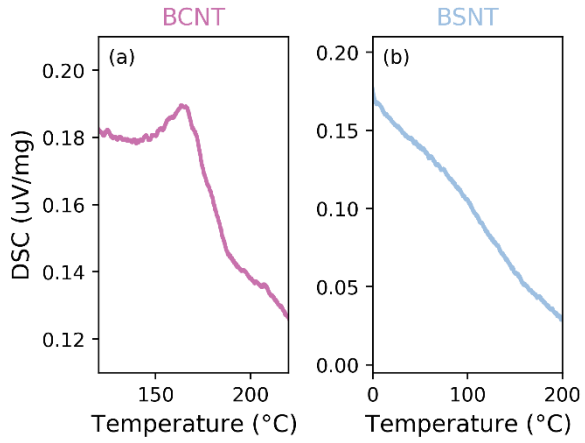

Figure S10: Differential scanning calorimetry as function of temperature. Endothermic peaks are observed for (a) $Ba_4Ca_2Nb_8Ti_2O_{30}$ at 170 °C, while no peak is observed for (b) $Ba_4Sr_2Nb_8Ti_2O_{30}$.

Polarisation- and Strain-Electric Field measurements

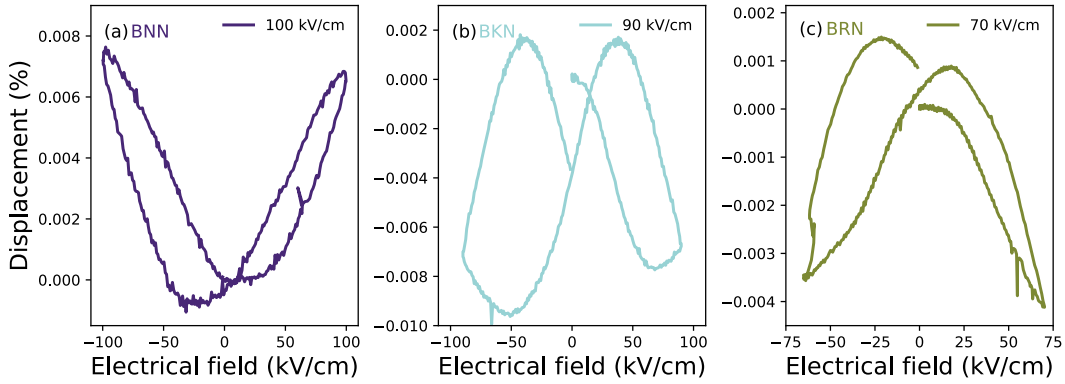

Figure S11: Strain-Electric field loops measured at 100 Hz and ambient temperature on ceramic (a) BNN at 100 kV/cm, (b) BKN 90 kV/cm and (c) BRN at 70 kV/cm.

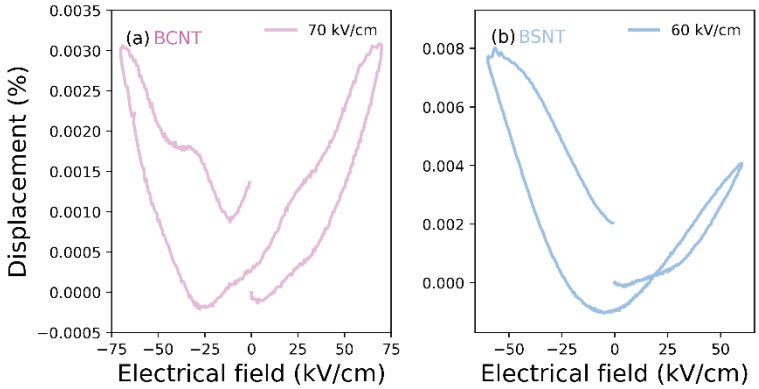

Figure S12: Polarisation-Electric field loops measured at 100 Hz and ambient temperature on ceramic (a) BCNT at 70 kV/cm and (b) BSNT at 60 kV/cm.

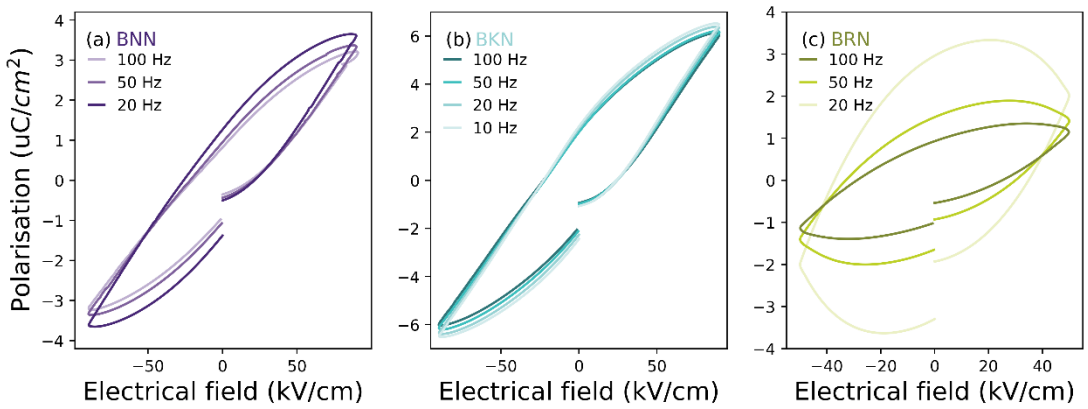

Figure S13: Polarisation-Electric field loops measured between 10-100 Hz and ambient temperature on ceramic (a) BNN at 70 kV/cm, (b) BKN at 70 kV/cm and (c) BRN at 50 kV/cm.

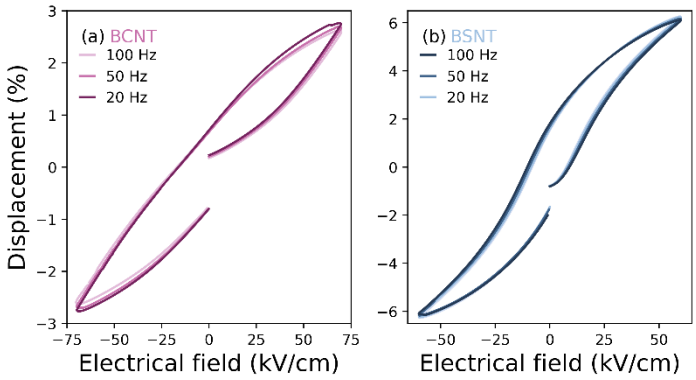

Figure S14: Polarisation-Electric field loops measured between 10-100 Hz and ambient temperature on ceramic (a) BCNT at 70 kV/cm and (b) BSNT at 60 kV/cm.

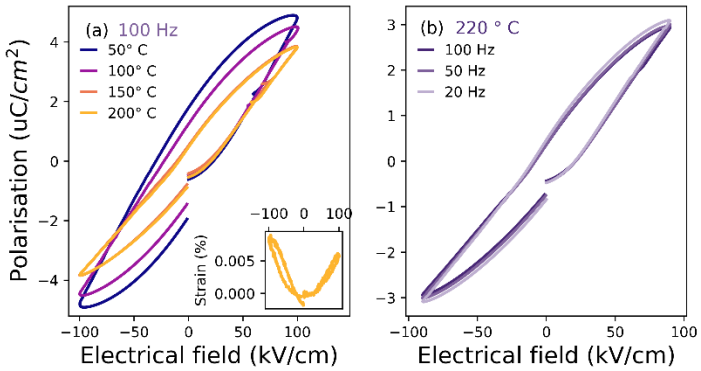

Figure S15: Polarisation-Electric field loops measured on ceramic BNN at (a) 100 Hz and 100 kV/cm at temperatures between 50 and 200 °C (Inset: strain-electric field loop at 200 °C) and (b) between 20-100 Hz at 90 kV/cm and 220 °C.

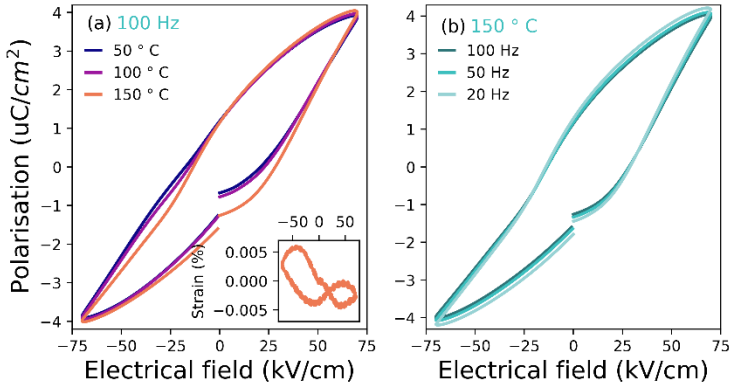

Figure S16: Polarisation-Electric field loops measured on ceramic BKN at (a) 100 Hz and 70 kV/cm at temperatures between 50 and 150 °C (Inset: strain-electric field loop at 150 °C) and (b) between 20-100 Hz at 70 kV/cm and 150 °C.

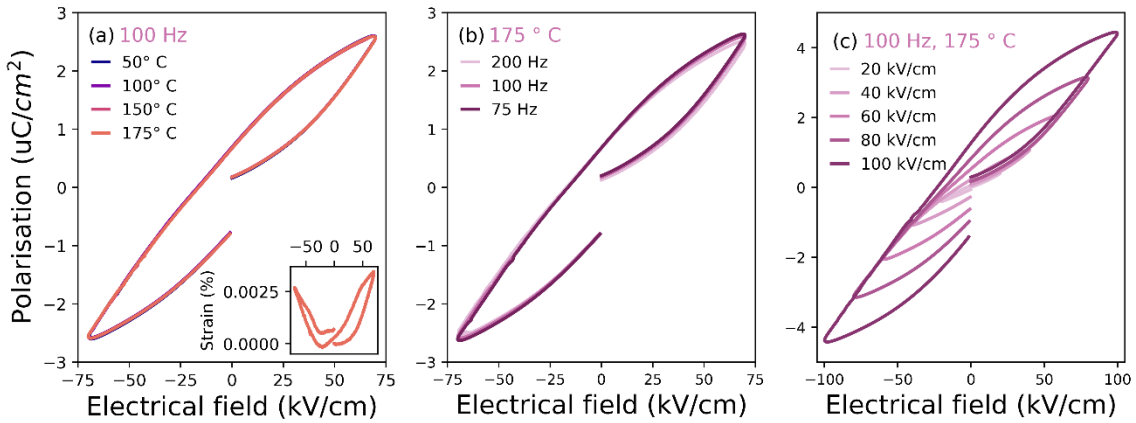

Figure S17: Polarisation-Electric field loops measured on ceramic BCNT at (a) 100 Hz and 100 kV/cm at temperatures between 50 and 175 °C (Inset: strain-electric field loop at 175 °C), (b) between 20-100 Hz at 100 kV/cm and 175 °C and (c) from 20-100 kV/cm at 100Hz and 175 °C.

Symmetry inequivalent configurations of cation site interchange

Table S5: Symmetry inequivalent configurations and their respective degeneracies in the supercell used for each system (M=Ca, Sr, Ba; R=Na, K, Rb).

R on A1 Site [%]	symmetry inequivalent configurations	degeneracy
100	1	1
75	2	128
50	3	336
25	14	896
0	10	70

Tabulated Structural Data from DFT

Table S6: Tabulated lattice parameters and Nb-O-Nb bond angles (representing tilting) in the c direction for $R_2MNb_5O_{15}$ materials with compositions with R=Ca and M=Na, K, Rb in the *P*4/*mbm* space group. The standard deviation in Nb-O-Nb corresponds to the averaged standard deviation of Nb-O-Nb angles within a single cell weighted by the probability of the configuration.

R=Ca (P4/mbm)	R on A1 [%]	a [Å]	b [Å]	c [Å]	<Nb-O-Nb (c) [°]	Std. dev.
M=Na	0	12.38	12.30	3.81	160.98	4.90
	25	12.43	12.29	3.80	159.51	3.80
	50	12.47	12.17	3.81	159.71	1.61
	75	12.21	12.47	3.79	161.59	4.54
	100	12.65	12.65	3.91	169.22	6.23
M=K	0	12.40	12.50	3.81	165.42	6.03
	25	12.33	12.50	3.81	164.91	5.83
	50	12.56	12.62	3.87	167.13	2.08
	75	12.42	12.46	3.82	164.27	6.36
	100	12.40	12.40	3.90	175.34	2.33
M=Rb	0	12.47	12.54	3.84	168.87	6.61
	25	12.40	12.65	3.83	167.19	5.60
	50	12.54	12.94	3.87	166.80	1.12
	75	12.64	12.49	3.84	163.84	5.48
	100	12.72	12.72	3.90	169.58	6.02

Table S7: Tabulated lattice parameters and Nb-O-Nb bond angles (representing tilting) in the c direction for $R_2MNb_5O_{15}$ materials with compositions with R=Sr and M=Na, K, Rb in the *P*4/*mbm* space group. The standard deviation in Nb-O-Nb corresponds to the averaged standard deviation of Nb-O-Nb angles within a single cell weighted by the probability of the configuration.

R=Sr (P4/mbm)	R on A1 [%]	a [Å]	b [Å]	c [Å]	<Nb-O-Nb (c) [°]	Std. dev.
M=Na	0	12.48	12.41	3.85	166.68	4.50
	25	12.44	12.48	3.83	165.06	3.87
	50	12.29	12.46	3.84	162.35	3.49
	75	12.36	12.46	3.82	164.31	2.19
	100	12.39	12.39	3.91	176.47	2.04
M=K	0	12.57	12.60	3.88	168.93	4.97
	25	12.56	12.55	3.87	167.39	4.34
	50	12.57	12.59	3.89	169.17	2.03
	75	12.52	12.53	3.86	166.98	3.80
	100	12.43	12.43	3.92	177.00	1.73
M=Rb	0	12.60	12.67	3.90	169.06	3.10
	25	12.59	12.62	3.88	167.85	4.19
	50	12.65	12.67	3.90	169.98	1.65
	75	12.60	12.61	3.88	167.42	4.04
	100	12.47	12.47	3.93	177.74	1.13

Table S8: Tabulated lattice parameters and Nb-O-Nb bond angles (representing tilting) in the c direction for $R_2MNb_5O_{15}$ materials with compositions with R=Ba and M=Na, K, Rb in the *P*4/*mbm* space group. The standard deviation in Nb-O-Nb corresponds to the averaged standard deviation of Nb-O-Nb angles within a single cell weighted by the probability of the configuration.

R=Ba (P4/mbm)	R on A1 [%]	a [Å]	b [Å]	c [Å]	<Nb-O-Nb (c) [°]	Std. dev.
M=Na	0.00	12.70	12.70	3.92	172.89	3.09
	25.00	12.68	12.67	3.91	170.55	3.35
	50.00	12.59	12.64	3.92	171.35	4.30
	75.00	12.58	12.62	3.90	169.36	3.75
	100.00	12.53	12.53	3.94	177.22	1.39
M=K	0.00	12.69	12.74	3.93	172.64	2.10
	25.00	12.71	12.69	3.93	172.16	2.72
	50.00	12.68	12.65	3.93	172.67	2.95
	75.00	12.63	12.68	3.92	171.71	2.33
	100.00	12.57	12.57	3.95	177.74	1.13
M=Rb	0.00	12.72	12.78	3.94	172.08	1.88
	25.00	12.75	12.73	3.93	171.74	2.25
	50.00	12.70	12.75	3.93	172.35	1.15
	75.00	12.69	12.74	3.93	171.66	1.67
	100.00	12.60	12.60	3.96	178.11	0.94

Table S9: Tabulated lattice parameters and Nb-O-Nb bond angles (representing tilting) in the c direction for $R_2MNb_5O_{15}$ materials with compositions with R=Ba and M=Na, K, Rb in the *P*4*bm* space group. The standard deviation in Nb-O-Nb corresponds to the averaged standard deviation of Nb-O-Nb angles within a single cell weighted by the probability of the configuration.

R=Ba (*P*4*bm*)	R on A1 [%]	a [Å]	b [Å]	c [Å]	<Nb-O-Nb (c) [°]	Std. dev.
M=Na	0	12.61	12.61	3.98	174.17	2.16
	25	12.61	12.60	3.95	172.22	3.34
	50	12.54	12.55	3.95	169.22	2.85
	75	12.45	12.47	4.00	172.43	4.28
	100	12.46	12.46	4.03	177.98	0.71
M=K	0	12.58	12.58	4.02	176.25	0.85
	25	12.57	12.57	4.02	176.18	1.30
	50	12.55	12.55	4.02	176.69	1.04
	75	12.53	12.53	4.01	174.40	1.81
	100	12.51	12.51	4.02	178.25	0.02
M=Rb	0	12.63	12.64	4.01	175.26	1.29
	25	12.61	12.62	4.01	175.17	1.75
	50	12.59	12.60	4.02	176.08	1.65
	75	12.58	12.58	4.02	175.08	1.69
	100	12.54	12.54	4.04	178.65	0.67

Phonon Dispersion Spectra of $R_2MNb_5O_{15}$

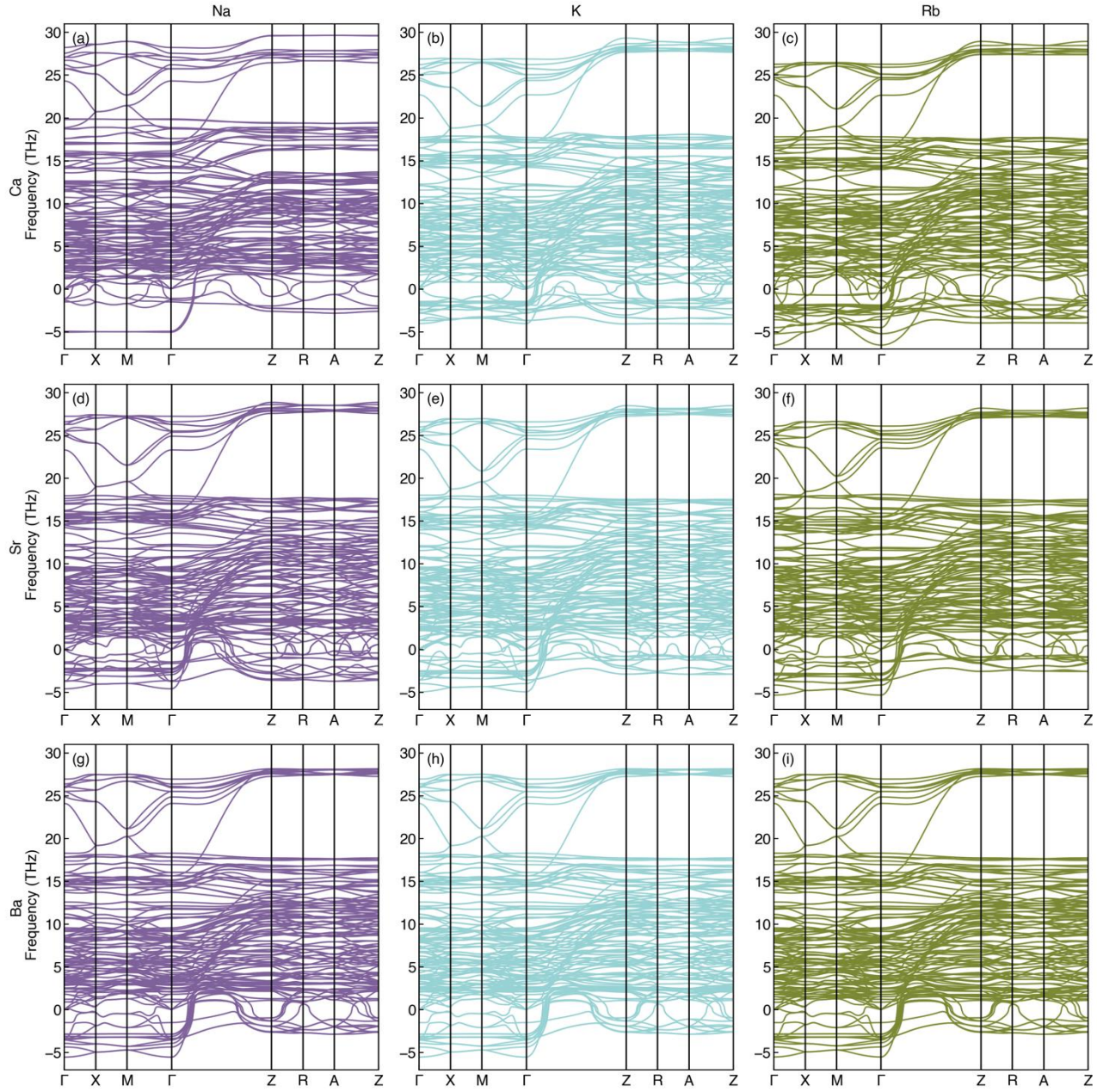

Figure S19: The phonon dispersion spectra for $R_2MNb_5O_{15}$ in the *P*4/*mbm* space group. (a-c) represent R=Ca, (d-f) R=Sr, (g-i) R=Ba where from left to right is M=Na, K, Rb.

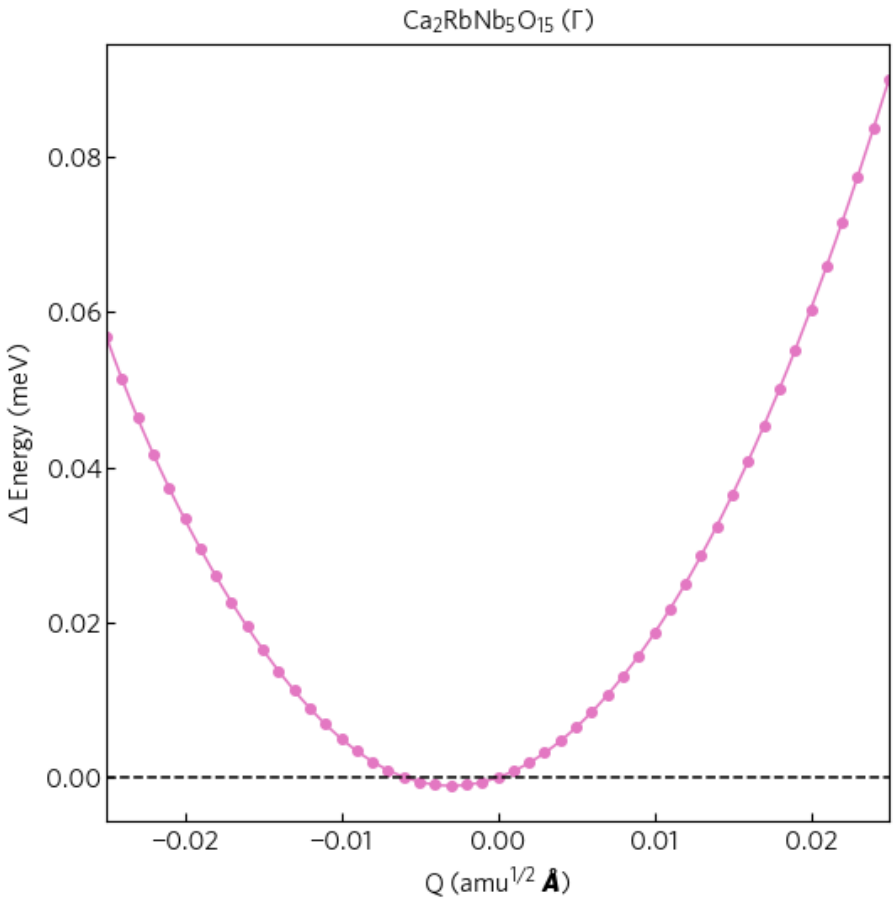

Figure S20: The calculated "mode mapping" of $Ca_2RbNb_5O_{15}$ at the Gamma point to a much tighter Q range showing the lack of a double well, yet a slight energy lowering off the starting configuration.

ΔE and ΔQ as a Function of Tolerance Factor

In Figure S, the anharmonic well depths (ΔE) and mode amplitude (ΔQ) at Γ **(**ΔE) for fully ordered stoichiometric compositions as a function of various TTB tolerance factors are given. The tolerance factors (TF_{A2} – A2 site tolerance factor, TF_{A1} – A1 site tolerance factor, TF_{TTB} – overall TTB tolerance Factor) taken from [1, 2]and are defined as:

$$TF_{A2} = \frac{R_{A2} + R_O}{\sqrt{23 - 12\sqrt{3}}(R_B + R_O)} \quad (1)$$

$$TF_{A1} = \frac{R_{A1} + R_O}{\sqrt{2}(R_B + R_O)} \quad (2)$$

$$TF_{TTB} = \frac{(TF_{A1} + 2TF_{A2})}{3} \quad (3)$$

Where R_{A2}, R_{A1}, R_B and R_O are the ionic radii for the A2, A1, B, and O site respectively.

In terms of ΔE, there is a negative correlation with TF_{TTB} and TF_{A2}. Within the A1 site, increasing R cation radii results in a larger ΔE.

For ΔQ, there is a weak positive correlation with TF_{TTB} and TF_{A2}. The A1 site has minimal impact on the mode amplitude, suggesting that the A2 site possesses the most influence over ΔQ.

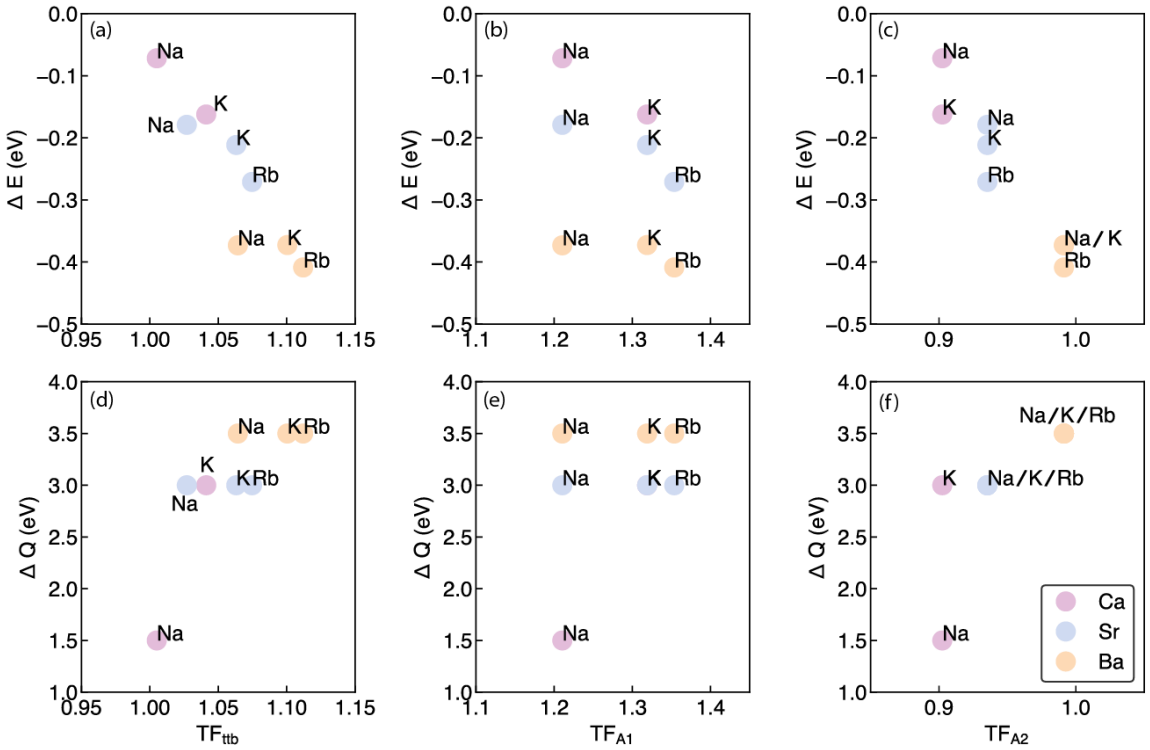

Figure S21: Anharmonic well depth (ΔE) (a-c) and Amplitude (ΔQ) (d-f) at Γ as a function of tolerance factor for (a,d) total, (b,e) A1 site, and (c,f) A2 site

Thermodynamics of Disorder

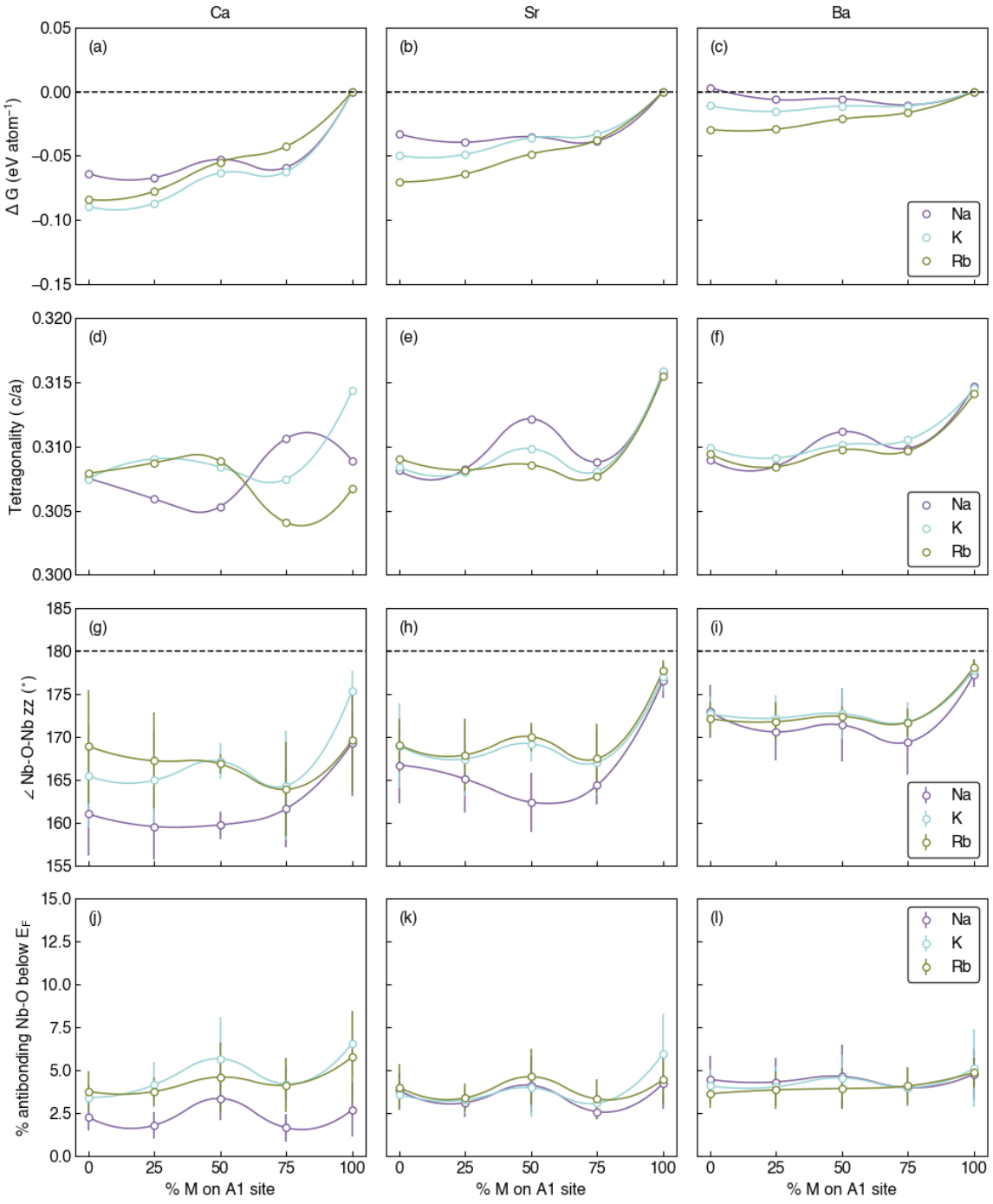

Figure S22: The thermodynamics of cation site disorder as a function of R (Ca, Sr, Ba) and M cation (Na, K, Rb) in $R_2MNb_5O_{15}$. In the top row (a,b,c) the Gibbs free energy of configuration is shown relative to the ordered state, the second row (d,e,f) shows the probabilistically averaged tetragonality, the third row (g,h,i) shows the influence of cation site disorder on the Nb-O-Nb bond angle in the c direction inferring octahedral tilting behaviour, and in the bottom row (j,k,l) show the antibonding nature of Nb-O interactions below the Fermi level (E_F). The error bars in (g,h,i) are calculated from the standard deviation of s angle towards all Nb-O-Nb angles in the unit cell, whilst the error bars in (j,k,l) are calculated from the standard deviation between inequivalent configurations.

References:

1. X. Zhu, M. Fu, M. C. Stennett, P. M. Vilarinho, I. Levin, C. A. Randall, J. Gardner, F. D. Morrison and I. M. Reaney, *Chem Mater*, 2015, **27**, 3250-3261.
2. N. Wakiya, J. K. Wang, A. Saiki, K. Shinozaki and N. Mizutani, *J Eur Ceram Soc*, 1999, **19**, 1071-1075.